NJC

Accepted Manuscript

This is an *Accepted Manuscript*, which has been through the Royal Society of Chemistry peer review process and has been accepted for publication.

Accepted Manuscripts are published online shortly after acceptance, before technical editing, formatting and proof reading. Using this free service, authors can make their results available to the community, in citable form, before we publish the edited article. We will replace this *Accepted Manuscript* with the edited and formatted *Advance Article* as soon as it is available.

You can find more information about *Accepted Manuscripts* in the Information for Authors.

Please note that technical editing may introduce minor changes to the text and/or graphics, which may alter content. The journal's standard Terms & Conditions and the Ethical guidelines still apply. In no event shall the Royal Society of Chemistry be held responsible for any errors or omissions in this *Accepted Manuscript* or any consequences arising from the use of any information it contains.

ROYAL SOCIETY OF CHEMISTRY

www.rsc.org/njc

Spectral, theoretical characterization and antifungal properties of two phenol derivatives Schiff base with an intramolecular hydrogen bond†

Alexander Carreño,[a,f*] Manuel Gacitúa,[b,g] Dayán Páez-Hernández,[a,f] Rubén Polanco,[d] Marcelo Preite,[c] Juan A. Fuentes,[d] Guido C. Mora,[e] Ivonne Chávez,[b,f] Ramiro Arratia-Pérez[a,f]

[a]Doctorado en Fisicoquímica Molecular, Center of Applied Nanosciences (CENAP), Universidad Andres Bello, Ave. República 275, Santiago, Chile, Zip Code: 8370146.

[b]Departamento de Química Inorgánica, Facultad de Química, Pontificia Universidad Católica de Chile.

[c]Departamento de Química Orgánica, Facultad de Química, Pontificia Universidad Católica de Chile.

[d]Facultad de Ciencias Biológicas, Laboratorio de Microbiología, Universidad Andres Bello, República 217, Santiago, Chile.

[e]Facultad de Medicina, Laboratorio de Microbiología, Universidad Andres Bello, República 590, Santiago, Chile

[f]Núcleo Milenio de Ingeniería Molecular para Catálisis y Biosensores, ICM, Chile

[g]Current address: Center of Applied Ecology and Sustainability (CAPES), Universidad Adolfo Ibáñez, Peñalolén, Chile

† Electronic supplementary information (ESI) available.

Abstract

Schiff bases show a wide variety of applications of great importance in medicinal research due to their range of biological activities. In this article we describe the electronic structure, optical, redox and antifungal properties of (*E*)-2-{[(2-aminopyridin-3-yl)imino]-methyl}-4,6-di-tert-butyl-phenol (**L1**) and (*E*)-2-{[(3-aminopyridin-4-yl)imino]-methyl}-4,6-di-tert-butyl-phenol (**L2**), two isomers phenol derivatives Schiff bases exhibiting a strong intramolecular hydrogen bond (O-H•••N). These compounds were characterized by their ^{1}H, HHCOSY, ^{13}C-NMR, FT-IR spectra, and by cyclic voltammetry. All the experimental results were complemented with theoretical calculations using density functional theory (DFT) and time-dependent DFT (TDDFT). The antimicrobial activity of the compounds described herein was assessed by determining the minimal inhibitory concentration (MIC) and by a modification of the Kirby-Bauer method. We tested *Salmonella enterica* serovar Typhi (*S.* Typhi, Gram-negative bacteria), *Cryptococcus* spp. (yeast), and *Candida albicans* (yeast). We found that neither **L1** nor **L2** showed antimicrobial activity against *S.* Typhi or *Candida albicans*. On another hand, **L2**, in contrast to **L1**, exhibited antifungal activity against a clinical strain of *Cryptococcus spp*. (MIC: 4.468 µg/mL) even better than ketoconazole antifungal medicaments. We mentioned above that **L1** and **L2** are isomer species, because the amino groups is in ortho-position in **L1** and in para-position in **L2**, however no significant differences were detectable by UV-vis, FT-IR, oxidation potentials and TDDFT calculations, but importantly, the antifungal activity clearly discriminated between these two isomers.

Keywords: Schiff base, intramolecular hydrogen bonds, DFT, antifungal, *Cryptococcus*

1. INTRODUCTION

Schiff base ligands derived from salicylaldehyde and substituted phenylene diamines containing an OH···N type hydrogen bonding known as Salen ligands have been studied due to the versatility of their electronic, chemical and biological properties.[1-3] Different metal complexes with Schiff base ligands have been synthesized and studied because of their ability to form stable complexes.[4] These complexes have also been used in analytical chemistry for the spectrophotometric determination of heavy metals, such as mercury ions[5,6] Besides, they were used as catalysts in chemical and photochemical reactions as well as many other applications. Schiff bases derived diamino pyridines with an -OH group in the ortho position relative to an azomethine group -C=N- have generated much interest due to the existence of an intramolecular hydrogen bond between the OH and the nitrogen atom of the azomethine group.[7,8] This research emphasizes the importance of an intramolecular hydrogen bond in such systems, which has been the subject of much investigation.

On the other hand, Schiff bases have been found to have important uses both in medicinal and pharmaceutical chemistry,[9-13] due to the highly versatile organic synthetic intermediates and the many heterocyclic ring systems[14,15] which show a broad range of biological activities, such as antibacterial,[16,17] antifugal,[18] and antiinflamatory.[19] The synthesis and antimicrobial activity of a series of Schiff bases derived from condensation of salicylaldehyde and diaminopyridine have been reported and demonstrated to inhibit the growth of fungi of clinical interest, such as *Candida Albicans* and *Cryptococcus neoformans*.[20]

With all that in mind, we aimed to investigate two isomer phenol derivatives, (*E*)-2-{[(2-aminopyridin-3-yl)imino]-methyl}-4,6-di-tert-butyl-phenol (**L1**) and (*E*)-2-{[(3-aminopyridin-4-yl)imino]-methyl}-4,6-di-tert-butyl-phenol (**L2**) (Scheme 1), each comprising a Schiff base and a potentially bioactive intramolecular hydrogen bond. The syntheses of compounds **L1** and **L2** were described by Kleij *et al*.[21, 22] In this work, a complete study of their electronic properties to understand the role of the hydrogen bond on its biological activities and molecular properties was performed.

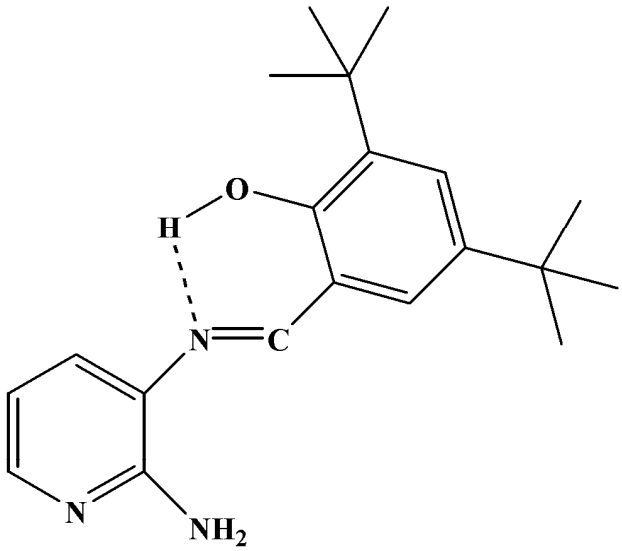

L1

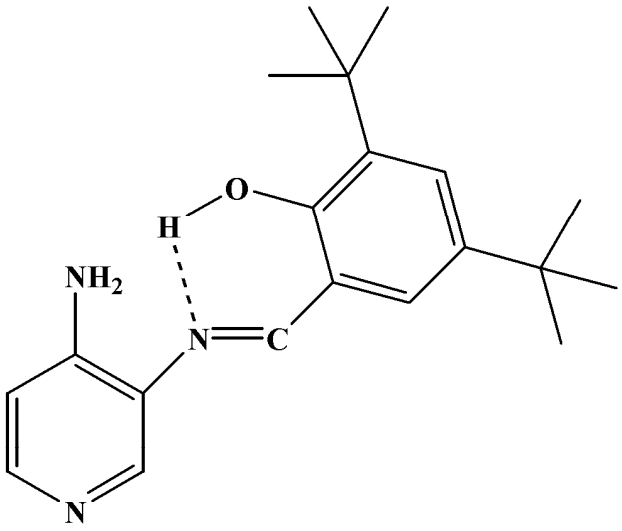

L2

Scheme 1. Structure of (*E*)-2-{[(2-aminopyridin-3-yl)imino]-methyl}-4,6-di-tert-butyl-phenol (**L1**) and (*E*)-2-{[(3-aminopyridin-4-yl)imino]-methyl}-4,6-di-tert-butyl-phenol (**L2**).

2. Experimental Section

2.1 Synthesis. All chemicals and solvents were purchased from Aldrich. All solvents were stored over the appropriate molecular sieves prior to use.

Synthesis of (*E*)-2-{[(2-aminopyridin-3-yl)imino]-methyl}-4,6-di-tert-butyl-phenol (L1) : was prepared by condensation of 2,3-diaminopyridine with 3,5-di-tert-butyl-2-hydroxi-benzaldehyde (in 20 mL of methanol), a modified template pathway.[21,22] The reaction was stirred for 24 h at room temperature and then filtered, and the precipitate was washed with methanol and diethyl ether. The yellow product was purified by crystallization, and the product was dried under vacuum. Yellow crystals suitable for X-Ray diffraction were obtained by slow evaporation of the solvent. Yield 70%.

^{1}H-NMR (400 MHz, $CDCl_3$, ppm): δ = 1.28 [s; 9H; -C(CH_3)$_3$], 1.47 [s; 9H; -C(CH_3)$_3$], 4.80 [bs; 2H; -NH_2], 6.72 [dd: J=7.6; 5.0 Hz; 1H; H2], 7.24 [m; 1H; H3], 7.26 [d: J=2.0 Hz; 1H; H5], 7.48 [d: J=2.0 Hz; 1H; H6], 8.01 [dd: J=5.0; 1.6 Hz; 1H; H1], 8.63 [s; 1H; H4], 13.03 [s; 1H; OH]. ^{1}H-NMR (400 MHz, DMSO-$_{d6}$, ppm): δ = 1.30 [s; 9H; -C(CH_3)$_3$], 1.43 [s; 9H; -C(CH_3)$_3$], 5.82 [bs; 2H; -NH_2], 6.66 [dd: J=7.6; 4.9 Hz; 1H; H2], 7.44 [dd; J=7.6; 1.3 Hz; 1H; H3], 7.41 [d: J=2.3 Hz; 1H; H5], 7.49 [d: J=2.3 Hz; 1H; H6], 7.90 [dd: J=4.9; 1.4 Hz; 1H; H1], 8.85 [s; 1H; H4], 13.22 [s; 1H; OH]. ^{13}C-NMR (400 MHz, CD_3Cl, ppm): δ= 29.42 (-C(CH_3)$_3$), 31.44 (-C(CH_3)$_3$), 34.22 (-C(CH_3)$_3$), 35.13 (-C(CH_3)$_3$), 114.39 (C10), 118.40 (C11),124.95 (C12), 126.96 (C4), 128.62 (C5), 130.71 (C9), 137.15 (C7), 141.08 (C1), 146.39 (C3), 153.32 (C2), 157.98 (C8), 164.91 (C6). FTIR (KBr,cm^{-1}): 3469 υOH , 3264 and 3136 υNH_2, 1609 υC=N, 1590 υC=C. UV/VIS: (dichloromethane, room temperature, c= 4.21x10^{-5} mol L^{-1}) λ(ε)=238 (33939 mol^{-1} dm^3 cm^{-1}), 279 (23569 mol^{-1} dm^3 cm^{-1}), 374 (22419 mol^{-1} dm^3 cm^{-1}). (Ethanol, room temperature, c= 4.21x10^{-5} mol L^{-1}) λ(ε)= 204 (53751 mol^{-1} dm^3 cm^{-1}), 237 (20556 mol^{-1} dm^3 cm^{-1}), 373 (12925 mol^{-1} dm^3 cm^{-1}). (Acetonitrile, room temperature, c= 4.21x10^{-5} mol L^{-1}) λ(ε)= 196 (75455 mol^{-1} dm^3 cm^{-1}), 236 (21702 mol^{-1} dm^3 cm^{-1}), 370 (12978 mol^{-1} dm^3 cm^{-1}). Anal. Calcd for $C_{20}H_{27}N_3O$: C, 73.84; H, 8.32; N, 12.92. Found C, 73.74; H, 11.93; N, 13.16.

Synthesis of (*E*)-2-{[(3-aminopyridin-4-yl)imino]-methyl}-4,6-di-tert-butyl-phenol (L2): 3,4-diaminopyridine (9.16 mmol) and 3,5-diterbutyl-2-hydroxi-benzaldehyde (9.16 mmol) were added to a round flask,[21,22] together with 15 mL of methanol at room temperature. The mixture was stirred for 24 hours, concentrated to a 60% of the original volume, and filtered. The resulting yellow solid (Yield 80%) was dried in a high vacuum line.

^{1}HNMR (400 MHz, $CDCl_3$, ppm): δ= 1.34 [s, 9H, $C(CH_3)_3$], 1.47 [s, 9H, $C(CH_3)_3$], 4.57 [bs, 2H, NH_2], 6.62 [d; J = 5.4 Hz; 1H; H2], 7.26 [d, J =2.1 Hz; 1H; H6], 7.49 [d; J=1.9 Hz; 1H; H5], 8.10 [d, J = 5.5 Hz; 1H; H1], 8.14 [s; 1H; H1], 8.65 [s, 1H; H4], 13.04 [s, 1H; -OH]. ^{1}H NMR (400 MHz, DMSO-d): δ= 1.26 [s, 9H, $C(CH_3)_3$], 1.39 [s, 9H, $C(CH_3)_3$], 5,94 [bs, 2H, NH_2], 6.68 [d, J = 5.4; 1H; H2], 7.37 [s; 1H; H6], 7.47 [s, 1H; H5], 7,92 [d, J =5.2; 1H; H1], 7,98 [s; 1H; H3], 8.81 [s, 1H; H4], 13.18 [s, 1H; -OH]. ^{13}CNMR (400 MHz, CD_3Cl): δ= 29.96; 31.86; 34.86; 35.51; 109.83 (C10); 118.82 (C11); 127.76 (12); 129.24 (C4); 129.61(C5); 137.60(C9); 139.45(C7); 141.60(C1); 147.15(C3); 148.70(C2); 158.54(C8); 165.35(C6).FTIR (KBr, cm^{-1}): 3643 and 3478 vOH; 3330 and 3205 v NH_2; 1668 vC=N; 1250 vC=C.UV/VIS: (ethanol, room temperature, c= 3.45x10^{-6} mol L^{-1}) λ(ε)= 224 (22756 mol^{-1} dm^3 cm^{-1}), 276(14760 mol^{-1} dm^3 cm^{-1}), 360 (14023 mol^{-1} dm^3 cm^{-1}); (dichloromethane, room temperature, c= 3.45x10^{-6} mol L^{-1}) λ(ε)= 231 (20569 mol^{-1} dm^3 cm^{-1}), 280 (15733 mol^{-1} dm^3 cm^{-1}), 365 (8275 mol^{-1} dm^3 cm^{-1}). Anal. Calcd. $C_{20}H_{27}N_3O$=: C, 73.84; H, 8.32; N, 12.92. Exp.: C, 74.09; H, 8.453; N, 13.17.

2.2 Characterization

The NMR spectra were recorded on a Bruker AVANCE 400 spectrometer operating at 400 MHz, at 25 ^{o}C. Samples were dissolved in either deuterated chloroform or dimethylsulfoxide, using tetramethylsilane as internal standard. IR spectra were obtained on a Perkin-Elmer 1310 or in a Bruker Vector-22 FT-IR spectrophotometer, in KBr discs. UV-vis spectra were performed using a Shimadzu Model UV-3101 PC UV-vis-NIR scanning spectrophotometer. For the electrochemical experiments, the working solution contained 0.01 mol/L of the respective compound with 0.1 mol/L tetrabutylammonium hexafluorophosphate ($TBAPF_6$, supporting electrolyte) in CH_3CN. Prior to each experiment, the working solution was purged with high purity argon, and an argon atmosphere was maintained during the whole experiment. A polycrystalline non-annealed platinum disc (2 mm diameter) was used as working electrode. A platinum gauze of large geometrical area, separated from the cell main compartment by a fine sintered glass, was used as counter electrode. All potentials quoted in this paper are referred to an Ag/AgCl electrode in tetramethylammonium chloride to match the potential of a saturated calomel electrode (SCE), at room temperature.

All electrochemical experiments were performed at room temperature on a CHI900B bipotentiostat interfaced to a PC running the CHI 9.12 software that allowed experimental control and data acquisition.

2.3 Antibacterial Activity

All the compounds were evaluated for their *in vitro* growth inhibitory activity against Gram-negative bacteria *Salmonella enterica* serovar Typhi STH2370 (*S.* Typhi), and the clinical yeasts *Candida albicans* and *Cryptococcus* spp. obtained from the Hospital Clínico de la Universidad de Chile, Santiago, Chile. Minimum inhibitory concentration (MIC) was obtained by broth dilution according .[23] The MIC is defined as the lowest concentration of the tested compounds at which no growth of the strain was observed after the incubation.[24] *S.* Typhi was previously grown in Luria-Bertani broth (Bacto peptone, 10 g/l; Bacto yeast extract, 5 g/l; NaCl, 5 g/l) at 37 °C with shaking to OD_{600} = 1.4 (stationary phase). Yeasts were previously cultured in Sabouraud broth (Bacto peptone, 10 g/L; glucose, 40 g/L; pH 5.6) at 28 °C without

shaking. [25] Stock solutions of the compounds were prepared in dimethyl sulfoxide (DMSO).[26] Further dilutions were performed with Bacto™ Tryptic Soy broth (pancreatic digest casein 17.0 g/l, papaic digest of soybean 3.0 g/l, dextrose 2.5 g/l, sodium chloride 5.0 g/l, dipotassium phosphate 2.5 g/l). The concentration range of the compounds tested was between 0.10 µg/ml and 200 µg/ml. The inoculated wells were then incubated at 37 °C for 24 h (bacteria), or 48 h (yeasts). A control, DMSO and ethanol 95% without any test compound, was included for each of the microorganisms. Only when the inhibition effects of the test compounds were distinguishable from the DMSO alone (or ethanol 95% in the case of chloramphenicol [**C1**]), the compound was considered to exhibit antimicrobial activity. The MIC values of the tested compounds were obtained as µg/ml. All the experiments were performed in triplicate. To qualitatively determine the antifungal activity of (*E*)-2-{[(2-aminopyridin-3-yl)imino]-methyl}-4,6-di-tert-butyl-phenol (**L1**) and (*E*)-2-{[(3-aminopyridin-4-yl)imino]-methyl}-4,6-di-tert-butyl-phenol (**L2**), a modification of the standard disk diffusion assay was used, with the following modifications. In brief, overnight cultures of *Cryptococcus* spp. were suitable diluted to seed 10^6 cfu in a Sabouraud plate (Sabouraud broth solidified by adding 15 g/L agar). Then, two metal rings were put on the plate prior to being filled with 100 µl of L1 (400 µg/ml) or 100 µl of L2 (400 µg/ml). When the agar plate absorbed **L1** and **L2**, the metal rings were removed. The yeasts were incubated 48 h at 37 °C. The diameters of the zones of growth inhibition were obtained as the average of two measurements along two axes passing through the center of the disk by duplicate. In all cases, diameters differed by no more than 1 mm.

2.4 Computational details

All structural and electronic properties were obtained using he Amsterdam Density Functional (ADF) code.[27] All molecular structures were fully optimized by an analytical energy gradient method as implemented by Verluis and Ziegler, [28,29] using the hybrid B3LYP functional [30] and the standard Slater-type-orbital (STO) basis set with triple-ζ quality double plus polarization functions (TZ2P) for all the atoms.[31] Frequency analyses were performed after the geometry optimization to corroborate the minimum and to compare with experimental infrared spectra. Time-dependent density functional theory (TDDFT),[32] employed at the same level of theory to calculate the excitation energies using in all cases the conductor-like screening model for

realistic solvents (COSMO),[33] three different media were considered in the calculation: acetonitrile, ethanol and dichloromethane to estimate the hydrogen bond stability and to visualize the conformational changes due to the solvent polarity, additionally the calculations were also performed in the gas phase.

The second part of the calculations focused on the determination of equilibrium oxidation and reduction potentials.[34,35] To define a computational protocol, it is helpful to refer to one of the thermodynamic cycles,[36] either oxidative or reductive, as illustrated in Figure 1.

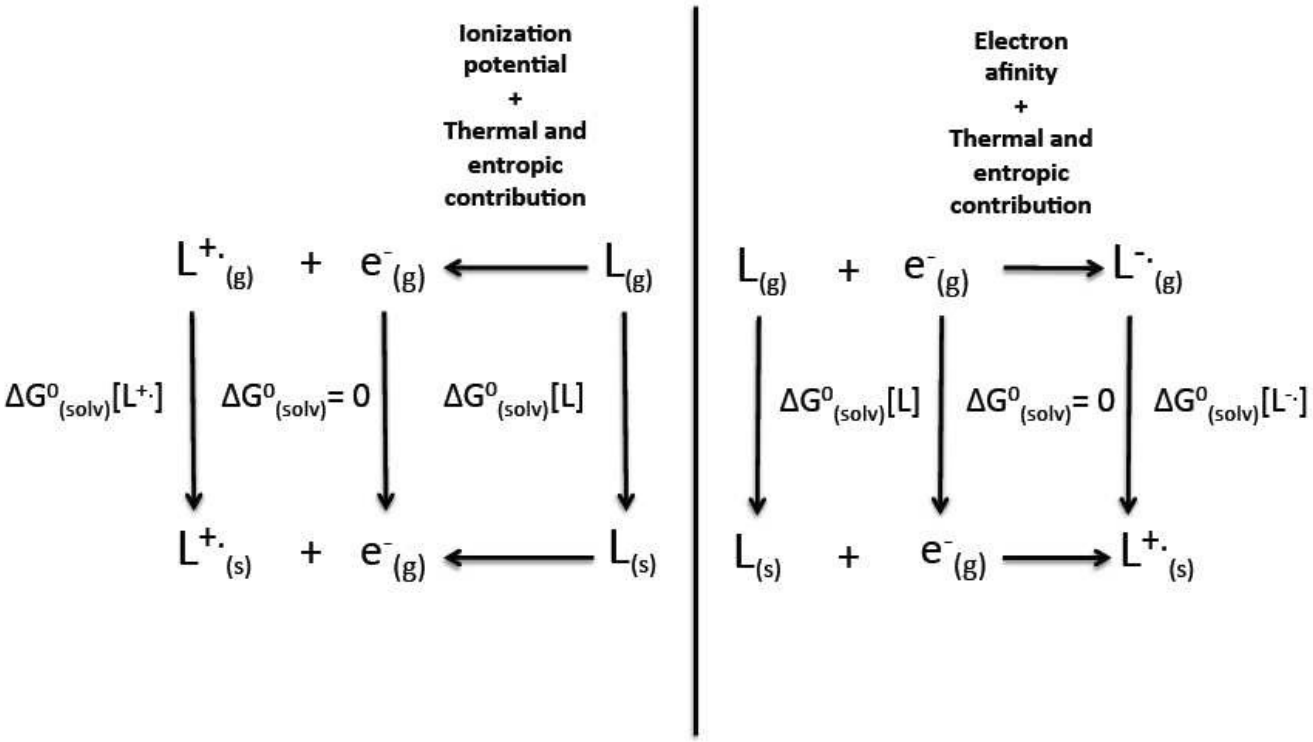

Figure 1. Thermodynamic cycles used in the computation of equilibrium oxidation and reduction potentials.

These cycles make clear the relationship between the condensed-phase free-energy changes associated with oxidation or reduction (the bottom legs of the illustrated cycles) and the relevant gas-phase processes.[37] In order to compute the free energy of ionization or electron attachment at 298 K (a typical temperature for the measurement of condensed phase oxidation and reduction potentials), the thermal contributions to the free energy at that temperature must be computed.[38] With this upper leg of the free-energy cycle in hand, it is

clear that the remaining connection between the gas phase and the condensed phase is simply the differential of the solvation free energies of the oxidized and reduced species for the process under consideration.[39] The absolute equilibrium oxidation or reduction free energy computed in the fashion just outlined, either generates or consumes a free electron. In practice, however, free electrons are not actual participants in most reactions. Instead, the electrons are consumed or generated, respectively, by another half-reaction. A typical half reaction is that which defines the standard hydrogen electrode (SHE) [equation 1].

$$H^{+}_{(ac)} + \bar{e} \longrightarrow 1/2\ H_{2\,(g)} \quad (1)$$

Another use of the SHE half reaction is as a reference for putting oxidation and reduction potentials on a convenient scale. Based on experiment, the free-energy change associated with Eq. (1) is -4.36 eV. To compute a given oxidation or reduction free energy relative to the SHE, one subtracts or adds, respectively, 4.36 eV to the free-energy change computed from the thermodynamic cycles in Figure 1 per electron transferred. Finally, relative oxidation and reduction potentials (E^{o}), are defined using following (equation 2):

$$E^{0} = -\Delta G^{0} / nF \quad (2)$$

where ΔG^{o} is the free-energy change relative to the SHE, n is the number of electrons consumed or generated in the half-reaction of interest, and F is the Faraday constant. The potential is expressed in volt units (for free energies expressed in some typical units, F=23.061 kcal /mol V = 96.485 kJ /mol V).

3. Results and Discussion

3.1 Synthesis, characterization and theoretical studies

(*E*)-2-{[(2-aminopyridin-3-yl)imino]-methyl}-4,6-di-tert-butyl-phenol (**L1**) was a yellow solid, obtained in 70% yield, and was prepared by the non-templated direct condensation of 2,3-diaminopyridine with 3,5-di-tert-buthyl-2-hydroxi-benzaldehyde, according to a previously described method.[22] The synthesis of (*E*)-2-{[(3-aminopyridin-4-yl)imino]-methyl}-4,6-di-tert-butyl-phenol (**L2**) was previously reported by Kleij *et al.*,[21] by condensation of 3,4-diaminopyridine with 3,4-di-tert-butyl-2-hydroxi-benzaldehyde, and was obtained in 80% yield. The FT-IR spectra of compounds **L1** and **L2** exhibited several bands between 2500 and 4000 cm^{-1}. The main absorption frequencies showed strong symmetric and asymmetric bands due to O-H vibrations at 3469 cm^{-1}, and two bands at 3264 and 3136 cm^{-1} assigned to -NH_2 for **L1**, and an O-H vibration at 3478 cm^{-1}, and two bands at 3330 and 33205 cm^{-1} assigned to -NH_2 for **L2**. For both compounds, the absorptions close to 1609 and 1590 cm^{-1} were assigned to C=N (azomethine group) and C=C stretchings, respectively, and have been previously reported for similar Schiff base.[40-43]

The ^{1}H NMR spectra (in $CDCl_3$) showed a strong intramolecular hydrogen bond signal for both (*E*)-2-{[(2-aminopyridin-3-yl)imino]-methyl}-4,6-di-tert-butyl-phenol (**L1**) and (*E*)-2-{[(3-aminopyridin-4-yl)imino]-methyl}-4,6-di-tert-butyl-phenol (**L2**) at about 13 ppm (numbering Scheme, and ^{1}HNMR spectra are given in Figures S1- S5, ESI†). Intramolecular H-bonding has been previously reported for similar compounds.[44,45] The -CH=N- azomethine proton (H4) appeared as a singlet at 8.63 ppm for **L1** and at 8.65 ppm for **L2**. The signals assigned to the *tert*-butyl groups appear at 1.47 and 1.28 ppm, and the aromatic protons of both rings at 7.50-6.70 ppm and 8.60-8.00 ppm for each compound, respectively. For **L1**, H2 proton appears at 6.72 ppm, H3 at 7.24 ppm and H1 at 8.01 ppm in the pyridine ring; for **L2**, H2 appears at 6.62 ppm, H3 at 8.10 ppm and H1 at 8.13 ppm. A signal assigned to the azomethine carbon atom (Figures S6-S8, ESI†) was observed at about 170 ppm for **L1** and **L2**.[46] ^{1}HNMR spectra in DMSO-$_{d6}$ for **L1** showed the intramolecular hydrogen-bonded proton at 13.22 ppm and amino

group protons at 5.82 ppm (Figures S9-S10, ESI†) and for **L2** at 13.18 ppm and 5.94 ppm, indicating the H-bond stability independent of solvent polarity. The C, H, N microanalyses are in agreement with the molecular formula $C_{20}H_{27}N_3O$.

In order to understand the electronic structures of (*E*)-2-{[(2-aminopyridin-3-yl)imino]-methyl}-4,6-di-tert-butyl-phenol (**L1**) and (*E*)-2-{[(3-aminopyridin-4-yl)imino]-methyl}-4,6-di-tert-butyl-phenol (**L2**), we employed DFT calculations using the approaches explained above. The first step in the calculations was a geometry optimization of the neutral compounds **L1** and **L2**. The energetic analysis show that **L1** was more stable than **L2** in 1.31 kcal/mol. Also the oxidized and reduced forms (Figures S11-S14, ESI†) with the aim to explain the redox properties.The main atom distances are in good agreement with the experimental crystallographic data reported for **L1** in our previous publication.[47] For **L2** a similar good correlation was found. Unfortunately the X-Ray crystal data for **L2** is not reported, but due to the similarities between both isomers we conclude that the geometrical differences are not significatives. Both compounds show an intramolecular hydrogen bond with an OH···N distance of 1.681 Å and 1.582 Å for **L1** y **L2**, respectively (Figure 2). In their neutral forms, the structures adopt an almost coplanar conformation, with a dihedral angle between the aromatic rings of 35.5º and 43.6º, respectively, for **L1** and **L2**. This coplanar configuration occurs due to the conjugation between both aromatic rings trough the azomethine -CH=N- double bond, which is the bridge between the rings. However, in the oxidized and reduced forms the azomethine bond partially reduced its order because of the reduction of the electronic population in the bonding orbital centered in the azomethine for the oxidized form, and due to the population of the antibonding orbital in the reduced form; that produced a break in the conjugation between both rings with the consequent increment of the dihedral angle between the rings. All that is summarized in Table 1 (Experimental values reported in Reference 47 appears between parenthesis), where it is possible to see the increment in the azomethine distance in both redox forms. In the same way, the calculated frequencies are in good agreement with the values observed in the FT-IR spectra for the most important functional groups in the similar compounds.[48] All the frequencies were positive which mean that the minimum was found. In general, there are not differences between the frequencies of both isomers, as is shown in Table 2.

Table 1. Geometrical parameters calculated for (*E*)-2-{[(2-aminopyridin-3-yl)imino]-methyl}-4,6-di-tert-butyl-phenol (**L1**) and (*E*)-2-{[(3-aminopyridin-4-yl)imino]-methyl}-4,6-di-tert-butyl-phenol (**L2**) in neutral, oxidized and reduced forms. All distances are in Å.

Molecule	d(N-H) H bond	d(O-H)	d(C=N) azomethine	d(C=N) ring	d(C-NH_2) amine	d(C-O)
L1	1.681(1.87)[a]	1.001(0.84)	1.289(1.29)	1.405(1.41)	1.379(1.357)	1.358(1.35)
$L1^{+\cdot}$	1.600	1.031	1.321	1.370	1.335	1.336
$L1^{-\cdot}$	1.537	1.050	1.374	1.374	1.396	1.373
L2	1.582	1.034	1.301	1.412	1.380	1.356
$L2^{+\cdot}$	1.534	1.053	1.317	1.372	1.344	1.325
$L2^{-\cdot}$	1.501	1.065	1.365	1.375	1.399	1.374

[a]. Experimental values reported by Carreño *et al.* [47] appears between parenthesis.

Abbreviations:

$L1^{+\cdot}$= cationic ; **$L1^{-\cdot}$**= anionic.

Table 2. Calculated frequencies (in cm^{-1}) for the main groups of (*E*)-2-{[(2-aminopyridin-3-yl)imino]-methyl}-4,6-di-tert-butyl-phenol (**L1**) and (*E*)-2-{[(3-aminopyridin-4-yl)imino]-methyl}-4,6-di-tert-butyl-phenol (**L2**).

IR-SPECTRUM	$\nu_s(NH_2)$	$\nu_{as}(NH_2)$	ν(OH)	ν(-CH=N-)
L1	3449	3554	3310	1553-1567
L2	3458	3569	3350	1562-1582

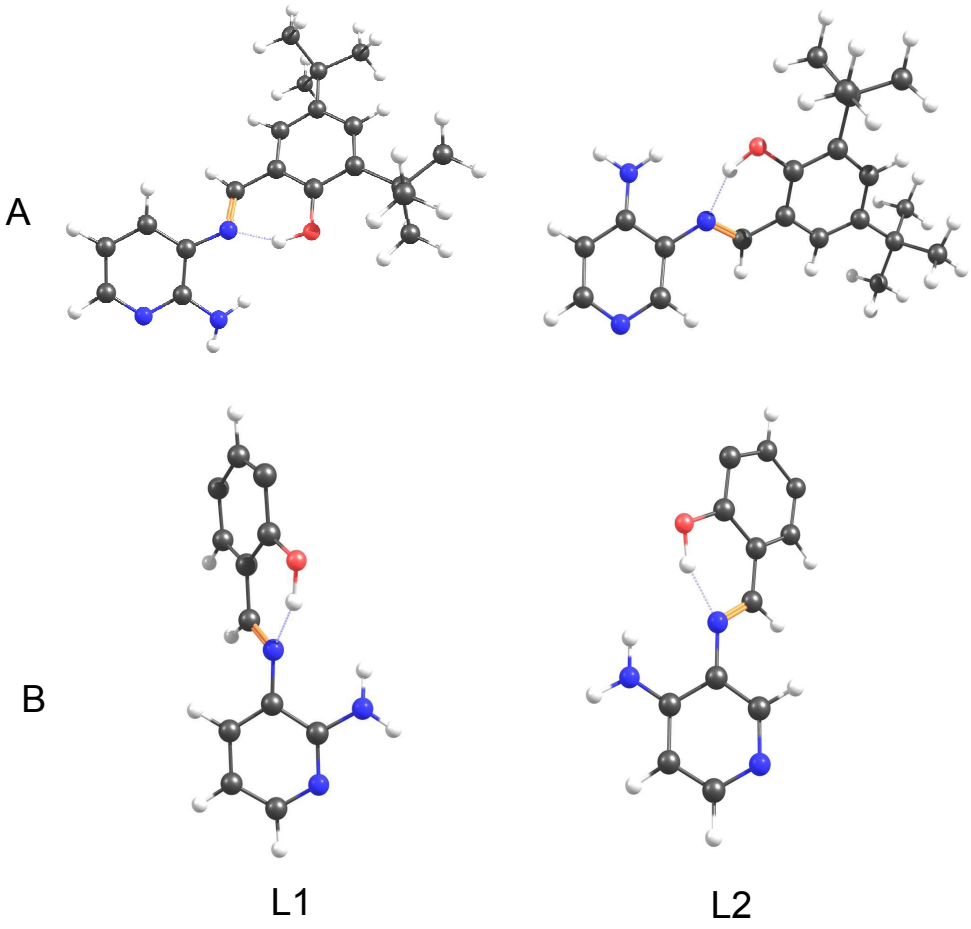

Figure 2. DFT optimized structure of compounds (*E*)-2-{[(2-aminopyridin-3-yl)imino]-methyl}-4,6-di-tert-butyl-phenol (**L1**) and (*E*)-2-{[(3-aminopyridin-4-yl)imino]-methyl}-4,6-di-tert-butyl-phenol (**L2**). The full structure is represented in **A** and the confomation between both rings around the azomethine group in **B** (tert-butyl groups are eliminated for simplicity).

The UV-vis spectra in dichloromethane and ethanol showed absorption bands centered at 375 nm and 200 nm (see Table 3) for **L1** and **L2**, which were assigned to n→π* (C=N) and π→π* transitions.[49,50] Time dependent density functional theory (TD-DFT) calculations were conducted to further elucidate the UV-vis transitions in three different solvents and in gas phase, as can be seen in Figures 3 and 4. The composition of the calculated transitions show that excitations associated to n→π* (-C=N-) band have a composition of 26% (HOMO-4 →

LUMO) and 74% (HOMO-3 → LUMO) for **L1** and 74% (HOMO-4 →LUMO) and 26% (HOMO-2 →LUMO) for **L2** in all the solvents and in gas phase. The bands assigned like π→π* transitions involve the HOMO→ LUMO for **L1** and **L2.** The comparison between the solvent spectra with the gas phase showed no significant shift in the UV-vis spectra when the solvent polarity changes.

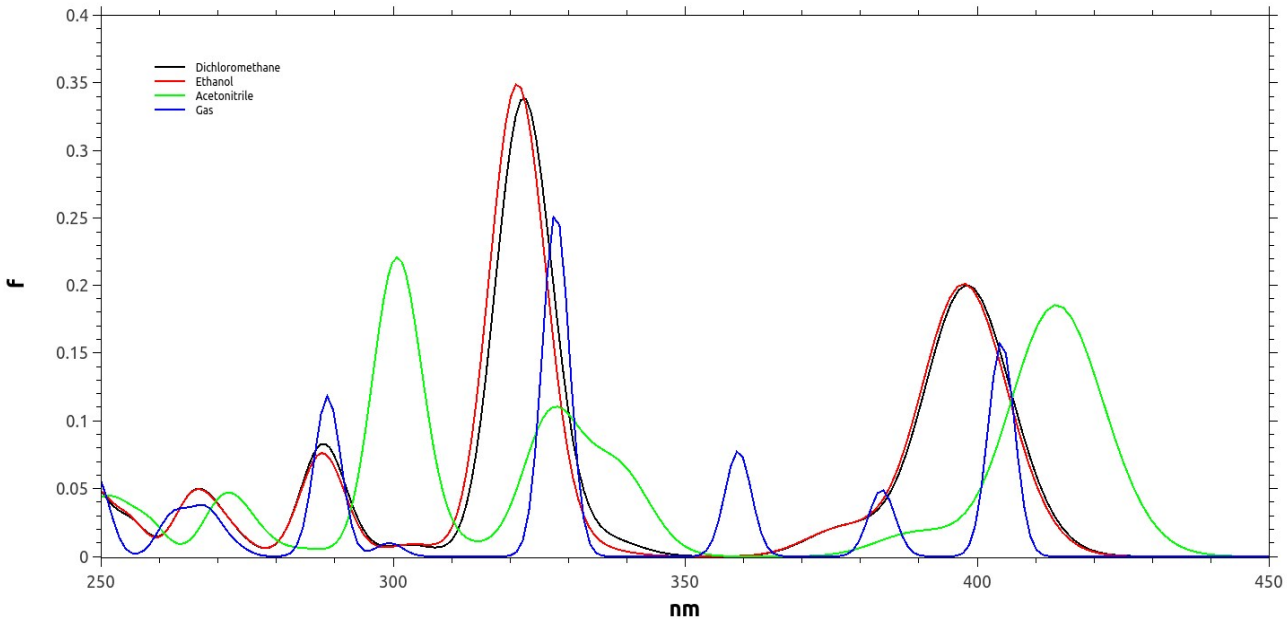

Figure 3. Calculated UV-vis absorption spectra for (*E*)-2-{[(2-aminopyridin-3-yl)imino]-methyl}-4,6-di-tert-butyl-phenol (**L1**) in different implicit solvents and gas phase.

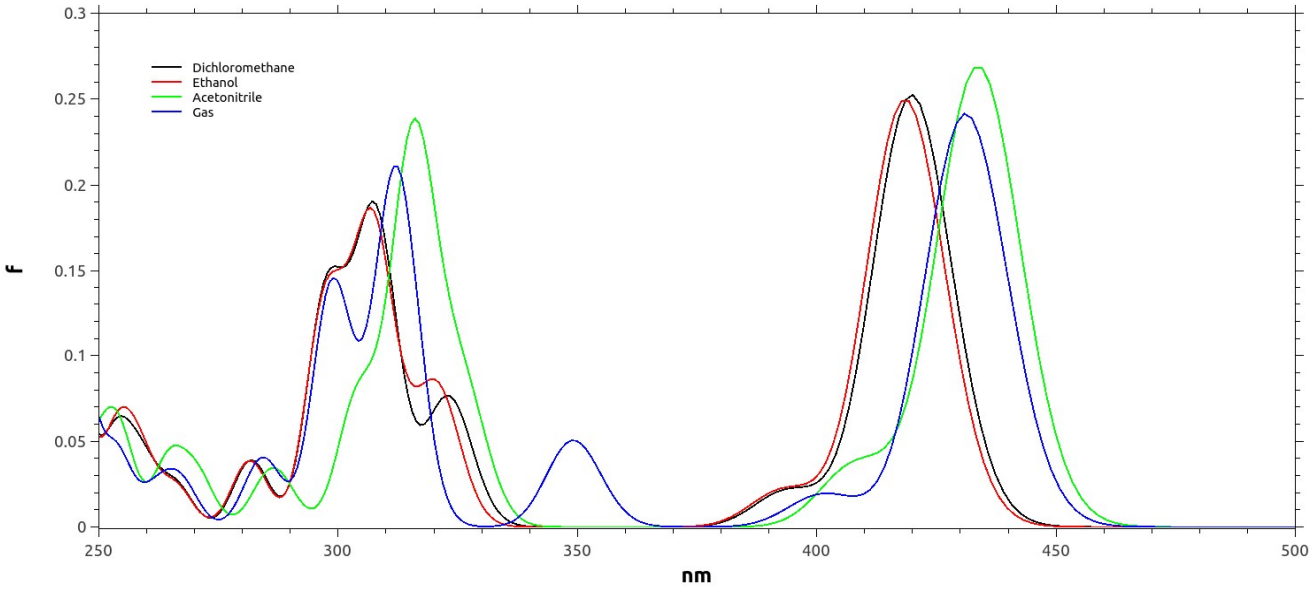

Figure 4. Calculated UV-vis absorption spectra for (*E*)-2-{[(3-aminopyridin-4-yl)imino]-methyl}-4,6-di-tert-butyl-phenol (**L2**) in different implicit solvents and gas phase.

On the other hand, previous studies about the luminescent properties in similar systems which contains the azomethine group concluded that the emission is a consequence of the rigidity of the structure which reduce substantially the vibronic relaxation.[51-53] In the present case compounds **L1** and **L2** exhibits no luminescent properties which is in agreement with the change in the configuration of the molecule when an excitation occurs. As was explained before the most important transitions in these molecules involve the LUMO orbital which have an antibonding character in the region of the azomethine group, it means that the excited state has not a double bond character in the region between both aromatic rings due to the population of this orbital, and like in the redox forms explained above the coplanar configuration is not retained. Then the excited state lost its rigidity and the probability of

emission is reduced. Optical excitation followed by a conformational changes in the C=C or N=N double bond had been described amply in the literature in photoisomerization studies.[54-57].

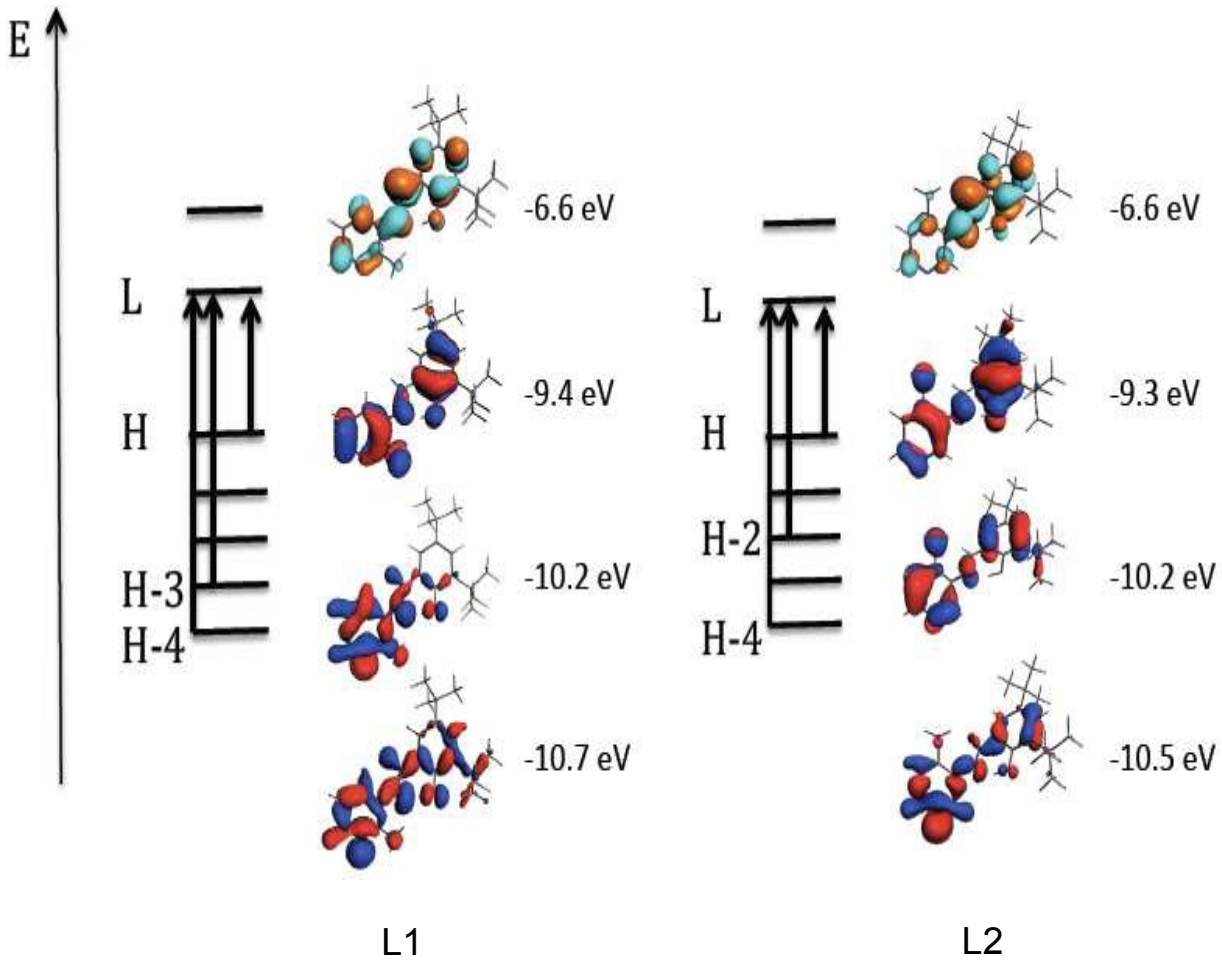

Figure 5. Qualitatively Molecular Orbital diagram for (*E*)-2-{[(2-aminopyridin-3-yl)imino]-methyl}-4,6-di-tert-butyl-phenol (**L1**) and (*E*)-2-{[(3-aminopyridin-4-yl)imino]-methyl}-4,6-di-tert-butyl-phenol (**L2**) with the most important electronic transitions.

Table 3. Experimental maximum wavelengths (nm) and Molar extinction coefficients (10^{-3} mol^{-1} dm^3). Calculated maximum wavelengths (nm), Energies (eV) and Nature of the electronic transitions for (*E*)-2-{[(2-aminopyridin-3-yl)imino]-methyl}-4,6-di-tert-butyl-phenol (**L1**) and (*E*)-2-{[(3-aminopyridin-4-yl)imino]-methyl}-4,6-di-tert-butyl-phenol (**L2**).

	λ_{exp}	ε	λ_{cal}	f ($x10^{-1}$)	Assiggnment
			L1		
ethanol	273	20.6	306	1.8	HOMO-4→ LUMO HOMO-3 →LUMO $n\rightarrow\pi^*$
	373	12.9	417	2.5	HOMO→ LUMO $\pi\rightarrow\pi^*$
dichloromethane	279	23.6	307	1.8	HOMO-4 →LUMO HOMO-3 →LUMO $n\rightarrow\pi^*$
	374	22.4	420	2.5	HOMO→ LUMO $\pi\rightarrow\pi^*$
			L2		
ethanol	276	14.8	320	3.4	HOMO-4 →LUMO HOMO-2 →LUMO $n\rightarrow\pi^*$
	360	14	395	1.9	HOMO→ LUMO $\pi\rightarrow\pi^*$
dichloromethane	280	15.7	322	3.4	HOMO-4→ LUMO HOMO-2 →LUMO $n\rightarrow\pi^*$
	365	8.3	398	2.0	HOMO→ LUMO $\pi\rightarrow\pi^*$

The electrochemical study consisted essentially on cyclic voltammetry experiments (Figure 6) in solutions containing the compounds (straight lines) compared against the same experiments done in solutions with supporting electrolyte only (dashed lines) for **L2**. The electrochemical study of **L1** was reported by Carreño *et al*.[22]

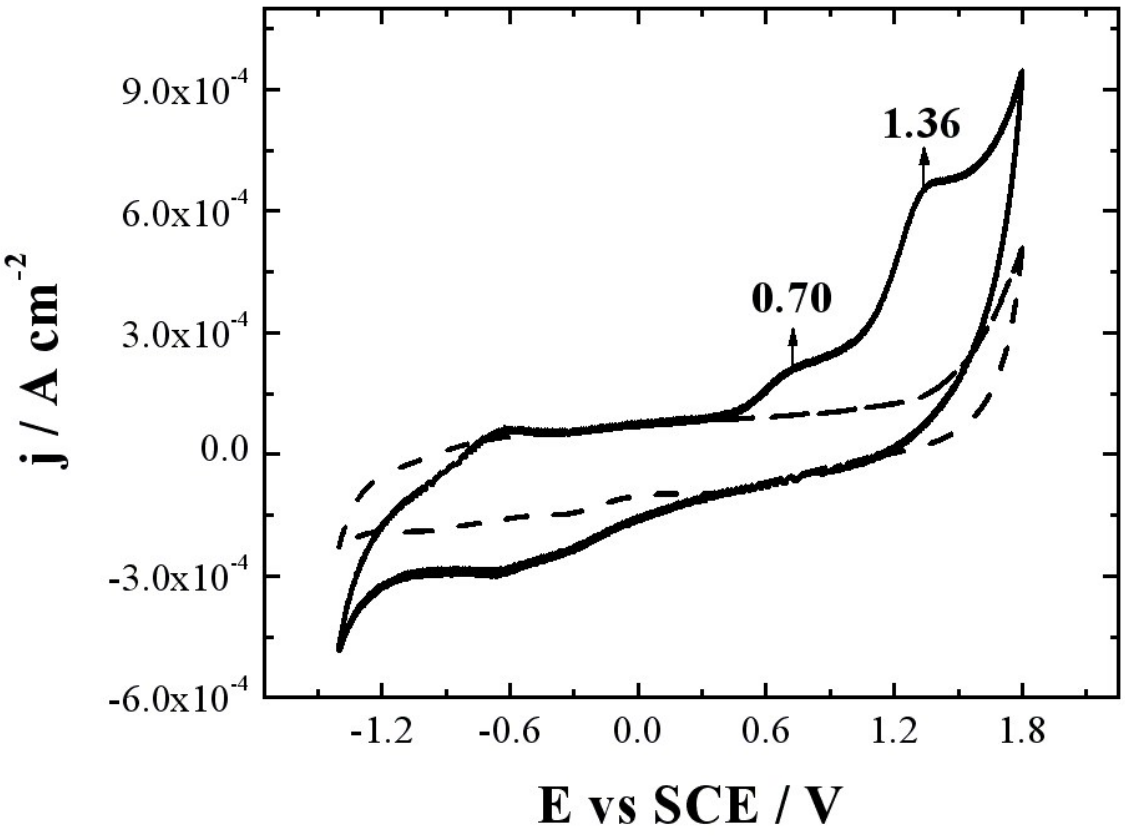

Figure 6. CV profiles of compound (*E*)-2-{[(3-aminopyridin-4-yl)imino]-methyl}-4,6-di-tert-butyl-phenol (**L2**) . Interface: Pt | 0.01 mol L^{-1} of compound + 0.1 mol L^{-1} of $TBAPF_6$ in anhydrous CH_3CN under an argon atmosphere. Scan rate: 200 mV s^{-1}.

At first glance, several signals where observed for **L2**. However, in order to describe processes and discard others a working-window study was firstly carried out. Hence, different potential range where used in order to check the dependence of each signal with the others, (Figure 7).

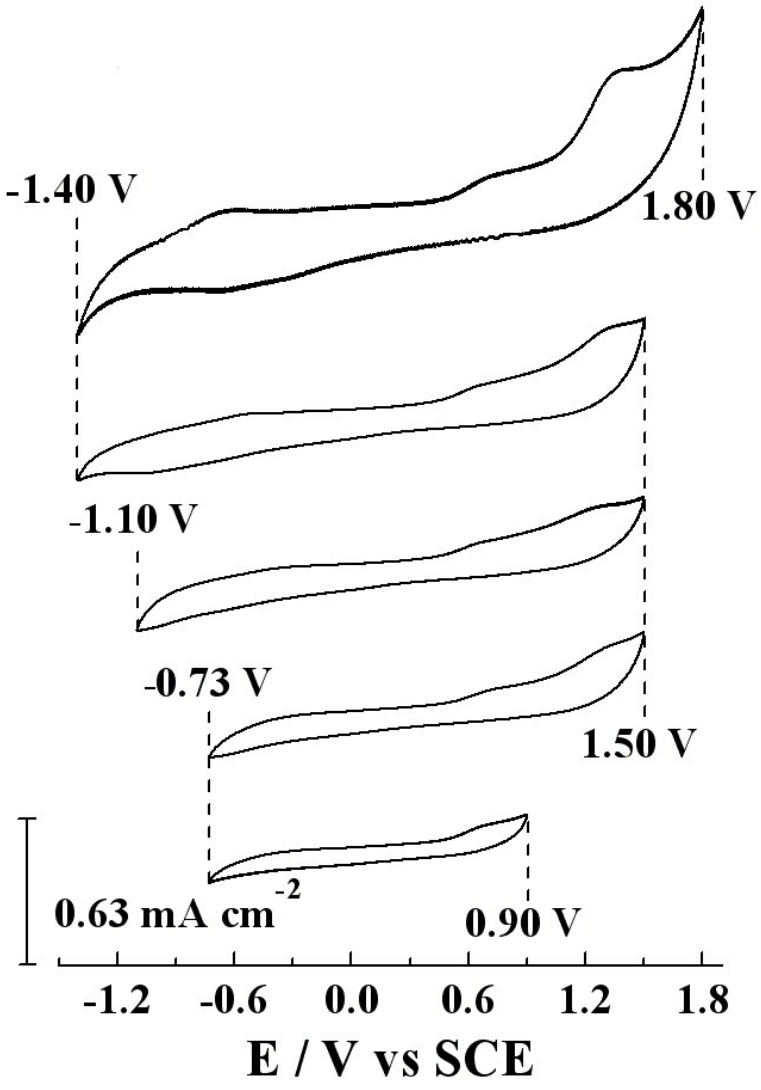

Figure 7. CV working-window study of compound (*E*)-2-{[(3-aminopyridin-4-yl)imino]-methyl}-4,6-di-tert-butyl-phenol (**L2**). Interface: same as Fig. 6.

As the working-window widens (from bottom to top) the signals start appearing showing their nature. Compound (*E*)-2-{[(3-aminopyridin-4-yl)imino]-methyl}-4,6-di-tert-butyl-phenol (**L2**) also presented a less intense reversible-like redox process when reaching the negative limit. However, it can be noticed that these processes appear only when reaching the widest limits

of potential, which proves that they are not necessarily related and might be attributed to secondary reactions of the molecule with the solvent or adsorption/desorption processes which is not interesting for the discussion. Nevertheless, **L2** also presents two irreversible oxidation processes with E_p values of 0.70 and 1.36 V which are attributed to the oxidation of the NH_2 and OH groups, respectively.[58,59] An evidence of these are the low values for the bond distances between C-NH_2 and C-O in the oxidized form shown in Table 1. The effect on the bond distances is much important in the amino group, suggesting that, a higher susceptibility of the amino group for the oxidation. These theoretical results are in agreement with the electrochemical experimental properties shown for aminophenol compounds reported by Salavaglione *et al*.[60,61] The theoretical calculations using the thermodynamic cycle presented above, predicts the same behavior for the oxidation process, showing 1.507 V and 1.572 V for (*E*)-2-{[(2-aminopyridin-3-yl)imino]-methyl}-4,6-di-tert-butyl-phenol (**L1**) and (*E*)-2-{[(3-aminopyridin-4-yl)imino]-methyl}-4,6-di-tert-butyl-phenol (**L2**), respectively. These values reproduce the same experimental tendency. Which is also corroborated in the framework of the hard and soft acids and bases (HSAB) principle proposed by Pearson.[62] An analysis of the HOMO- LUMO gap shows that **L1** has a value of hardness $\eta=1/2(\mathrm{HOMO}-\mathrm{LUMO})$ lower than **L2** (1.31 vs 1.37, respectively) which confirm that **L1** is oxidized more easily.[22] With respect to reduction only the compound **L1** showed no electrochemical reversible peak potentials, but an important irreversible reduction process at -1.78 V, which is attributed to an intramolecular reductive coupling of the azomethine group, which involves a self-protonation reaction.[63, 64] That is presumably related with the reduction of the N-H bond distance (H of the intramolecular hydrogen bond) found in the reduced form in both molecules in the calculations. In those reactions, the phenolic hydroxyl group acts as a proton donor, and its reductive value depends on the solvent used and on the structure of the Schiff base.

Summarizing, compound (*E*)-2-{[(2-aminopyridin-3-yl)imino]-methyl}-4,6-di-tert-butyl-phenol (**L1**) exhibits a simpler voltammetric spectrum than compound (*E*)-2-{[(3-aminopyridin-4-yl)imino]-methyl}-4,6-di-tert-butyl-phenol (**L2**) and both molecules share irreversible oxidation processes at different E_p values. However, the reduction of **L2** was not observed in the experiment. The potential difference between both compounds indicates that **L1** is more easily oxidized than **L2.** In the case of the reduction potential the calculations appear more deviated with respect to the experimental values obtaining, -0.937 V and -0.891 V for **L1** and

L2, respectively. In this particular case, it is important to provide a good description of the intramolecular hydrogen bond because this interaction is fundamental in the reduction processes, as explained above. Then we think that the level of theory used in the present work describe well the most important part of the spectroscopic properties obtained experimentally and for the particular case of the reduction potential it is necessary to study deeply the role of the intramolecular hydrogen bond. Also, the possibility of a self-protonation and its effect in the electrochemical properties of these molecules cannot be discarded.

3.2 Antibacterial activities

Some compounds showing substituted imidazoles (e.g ketoconazole) exhibit antifungal properties by inhibiting the cytochrome P450-dependent, 14 α-demethylase, a key enzyme in the synthesis of ergosterol.[66] The ergosterol is the main sterol in most fungal cells membranes. Other compounds, such as the Schiff bases (e.g chitosane-derives Schiff base),[11] also exhibit antifungal and antibacterial properties. [67] In order to test the potential antimicrobial activity of (*E*)-2-{[(2-aminopyridin-3-yl)imino]-methyl}-4,6-di-tert-butyl-phenol (**L1**) and (*E*)-2-{[(3-aminopyridin-4-yl)imino]-methyl}-4,6-di-tert-butyl-phenol (**L2**), we determined the minimal inhibitory concentration (MIC) against *Salmonella enterica* serovar Typhi (*S.* Typhi), a Gram-negative that produces the typhoid fever in humans; [68] and clinical strains of *Candida albicans* and *Cryptococcus* spp., two yeasts involved in opportunistic infections in humans, some of them with death risk. [69] The results of antimicrobial analysis are shown in Table 4. Compounds with low MIC exhibit better antimicrobial activity. With respect to *S.* Typhi, we observed that none of the tested compounds exerted an antibacterial effect, with the exception of chloramphenicol (**C1**, control), a known antibacterial antibiotic used as an internal control. In the case of *Candida albicans*, we found that ketoconazole (**K1**, control) [70] exhibited an antifungal activity as expected (MIC: 1.115 μg/ml). In contrast, neither **L1** nor **L2** presented antifungal effects in this strain. On the other hand, we obtained different results with *Cryptococcus* spp. We observed that the *Cryptococcus* spp. strain used in this work was resistant to **K1**. This phenotype was already been reported and corresponds to approximately 13.1% of the *Cryptococcus* spp. strains usually analyzed.[71-76] Interestingly, **L2** presented a noteworthy antifungal activity against this same strain of *Cryptococcus* spp. (MIC: 4.468 μg/ml), strongly suggesting that **L2** exerts its antifungal effect through a different mechanism

compared with **K1**. Furthermore, in this case, **L2** appeared to be a better antifungal compared with **L1**, and even better compared with the commercial **K1** under the tested conditions and with the strains used. Figure 8 shows that the inhibition growth halos obtained with **L2** (2.61 cm) are evidently larger than the inhibition growth halos obtained with **L1** (1.21 cm) when *Cryptococcus* spp. was grown in agar plates, supporting the observations with the MICs. Thus, the best antifungal effect achieved with **L2** compared with **L1** strongly suggests that changes in the amine position of pyridine ring affect the biological effects of these compounds. In support of this hypothesis, when we tested the antifungal effect of **L2** in $Re(CO)_3^+$ complex, where the nitrogen pyridine is coordinated with the metal, we observed the loss of the antifungal effect (data not shown). [77] Altogether, these observations suggest that other changes in the amine position of pyridine ring or even changes in other substituents in the phenol ring conceivable could affect and improve the antifungal activity of **L2**. However, experimental research is necessary to determine which substitutions will work in this sense.

Table 4. Minimal inhibition concentration (μg/ml) of tested compounds.

	Bacteria	Yeasts	
	S. Typhi	*Candida albicans*	*Cryptococcus* spp.
C1	3.125	ND	ND
L1	-	-	-
L2	-	-	4.468
K1	-	1.115	-

- : The inhibition was indistinguishable from the vehicle (DMSO) alone

ND: Not determined

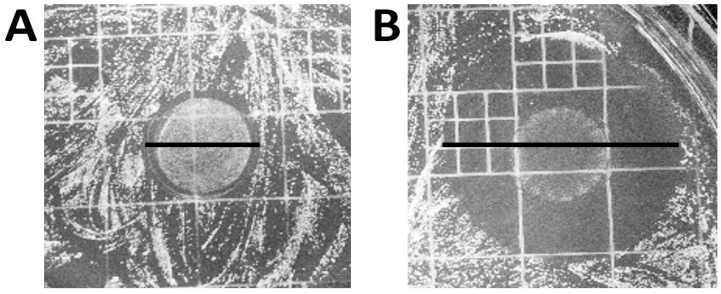

Figure 8. Inhibition growth halos of *Cryptococcus* spp. in presence of (*E*)-2-{[(2-aminopyridin-3-yl)imino]-methyl}-4,6-di-tert-butyl-phenol (**L1**) or (*E*)-2-{[(3-aminopyridin-4-yl)imino]-methyl}-4,6-di-tert-butyl-phenol (**L2**). The black horizontal lines delimits the inhibition growth halos in presence of A) **L1** (1.21 cm), or B) **L2** (2.61 cm).

4. Conclusions

The compounds (*E*)-2-{[(2-aminopyridin-3-yl)imino]-methyl}-4,6-di-tert-butyl-phenol (**L1**) and (*E*)-2-{[(3-aminopyridin-4-yl)imino]-methyl}-4,6-di-tert-butyl-phenol (**L2**) are Schiff bases isomers which presenting an intramolecular hydrogen bond synthesized and characterized by both experimental and theoretical studies and we have investigated their antimicrobial properties.

The presence of an intramolecular hydrogen bond for both compounds **L1** and **L2** were confirmed by ^{1}HNMR showing a strong peak at approximately 13 ppm in $CDCl_3$ and DMSO-d6, which is evidence of the intramolecular H-bond stability being independent of solvent polarity.

The electronic transitions computed by TD DFT method, including COSMO approximation, are in good agreement with the experimental spectra. The electronic studies showed that the absorption band assignment $\pi \rightarrow \pi^*$ is dominated by the HOMO→LUMO transition, with -OH group involvement. Also, computational studies and UV-vis spectra in different solvents confirm the stability of the hydrogen bond. Voltammetric peaks at 1.27 V for **L1**, and at 0.70 V and 1.36 V for **L2**, were observed and attributed to the oxidation of the amino and hydroxyl groups. These results are consistent with the theoretical studies.

In addition, we observed that (*E*)-2-{[(2-aminopyridin-3-yl)imino]-methyl}-4,6-di-tert-butyl-phenol (**L1**) and (*E*)-2-{[(3-aminopyridin-4-yl)imino]-methyl}-4,6-di-tert-butyl-phenol (**L2**) exerted no effect on a representative strain of Gram (-) bacteria. On the other hand, only **K1** (ketoconazole) affected *Candida albicans*, whereas again **L1** and **L2** exerted no effect. Surprinsingly, **L2** exhibited a MIC of 4.468 µg/ml and the inhibition growth halos, with a clinical strain of *Cryptococcus* spp. resistant to **K1**, whereas **L1** exerted no effect. To elucidate whether the pyridine nitrogen play a role in the antifungal activity of **L2**, compared to **L1**, escapes from the aims of this work.

Acknowledgements

Funded by Project RC120001 of the Iniciativa Científica Milenio (ICM) del Ministerio de Economía, Fomento y Turismo del Gobierno de Chile; *UNAB-DI-28-10/I project; Fondecyt 1150629, 11140294, 11121506, 1141138* and Núcleo UNAB Grant DI-22-12/N. We are grateful to Dr. Maria A. del Valle (UC) for instrumental facilities and Dr. Juan Manuel Manríquez (UBO) for valuable discussions. We thank B.A. Alfonso Inzunza G. for his help with the English translation.

Supporting Information

Supplementary data associated with this article can be found, in the online version.

References.

1. K.C. Gupta; A.K. Sutar, *Coord. Chem. Rev.* 2008, **252**, 1420

2. A. Prakash; D. Adhikari, *Int. J. Chem.* 2011, **3**, 1891

3. M. Holbach; X. Zheng; C. Burd; C.W. Jones; M. Weck, *J. Org. Chem*. 2006, **71**, 2903

4. S. Kumar; D. Nath Dhar; P.N. Saxena, *J. SCI. IND. RES*. 2009, **68**, 181

5. S. Kumari; G.S. Chauhan, *Appl. Mater. Interfaces*, **2014**, ***6,*** 5908

6. A.R. Fakhari; A.R. Khorrami; H. Naeimi, *Talanta* 2005, **66**, 813

7. L.K.W. Henri; J. Tagenine; B.M. Gupta, *Indian J. Chem*. 2001, **40A**, 999

8. A.O. Sobola; G.M. Watkins; B. Van Brecht, *S. Afr. J. Chem*. 2014, **67**, 45

9. A. Kathiravan; K. Sundaravel; M. Jacob; G. Dhinagaran; A. Rameshkumar; D.A. Ananth; T. Sivasudha, *J. Phys. Chem. B*, 2014, **118**, 13573

10. A. Kajal; S. Bala; S. Kamboj; N. Sharma; V. Saini, *Journal of catalysts*, 2013, 1

11. C.M. da Silva; D.L da Silva; L.V. Modolo; R.B. Alves; M.A. de Resende; C.V.B. Martins.; A. de Fatima, *Journal of Advanced Research*, 2011, **2**, 1

12. S. Arulmurugan; H.P. Kavitha; B.R. Venkatraman, *Rasayan J. Chem*. 2010, **3**, 385

13. A.R. Patil; K.J. Donde; S.S. Raut; V.R. Patil; R.S. Lokhande, *J. Chem. Pharm. Res.*, 2012, **4**, 1413

14. H.H. Elssa, *Organic Chem Curr Res*, 2013, **2**, 1

15. H. Kumar; R.P. Chaudhary, *Der Chemica Sinica*, 2010, **1**, 55

16. M. Shibata; T. Tanimoto; H. Kandori, *J. Am. Chem. Soc*. 2003, **125**, 13312

17. L. Li; Z. Li; K. Wang; S. Zhao; J. Feng; J. Li; P. Yang; Y. Liu; L. Wang; Y. Li; et al., *J. Agric. Food Chem.* 2014, **62**, 11080

18. M.B. Halli; R.S. Malipatil; R.B. Sumathi; K. Shivakumar, *Scholars Research Library Der Pharmacia Lettre*, 2013, **5**, 182

19. M. Gulcan; M. Sonmez; I. Berber, *Turk J. Chem.* 2012, **36**, 189

20. D. Kunal; K.D. Patel; F.J. Scarano; M. Kondo; R.A.R. Hurta; C.C. Neto, *J. Agric. Food Chem*. 2011, **59**, 12864

21. A.W. Kleij; D.M. Tooke; A.L. Spek; J.N.H. Reek, *Eur. J. Inorg. Chem*. 2005, **11**, 4626

22. A. Carreño; A. Vega; X. Zarate; E. Schott; M. Gacitua; N. Valenzuela; M. Preite; J.M. Manriquez; I. Chavez, *Quim. Nova*, 2014, **37**, 584

23. J.H. Rex; M.A. Pfaller; T.J. Walsh; V. Chaturvedi; A. Espinel-Ingroff; M.A. Ghannoum; L.L. Gossey; F.C. Odds; M.G. Rinaldi; D.J. Sheehan; D.W. Warnock, *CLIN. MICROBIOL. REV*. 2001, 643

24. M. Cuenca-Estrella; C.B. Moore; F. Barchiesi; J. Bille; E. Chryssanthou; D.W. Denning et al., *Clinical microbiology and infection : the official publication of the European Society of Clinical Microbiology and Infectious Diseases*. 2003, **9**, 467

25. A.W. Bauer; C.E. Roberts Jr.; W.M. Kirby, *Antibiotics annual*. 1959; **7**, 574

26. H. Vanden Bossche; P. Marichal; J. Gorrens; M.C. Coene, *British journal of clinical practice Supplement*. 1990, **71**, 41

27. Amsterdam Density Functional (ADF) Code; Vrije Universiteit: Amsterdam, 2007.

28. L. Verluis; T. Ziegler, *J. Chem. Phys*. 1988, **88**, 322

29. S.H. Vosko; L. Milk; N. Nusair, *J. Phys.* 1980, **58**, 1200

30. A.D. Becke, *J. Chem. Phys.* 1993, **98**, 5648

31. D. Paez-Hernandez; J. Murillo-Lopez; R. Arratia-Perez, Organometallics, 2012, **31**, 6297

32. F. Kootstra; P.L. Boeij; J.G. Snijders, *J. Chem. Phys*. 2000, **112**, 6517

33. P. Romaniello; P.L. de Boeij, *Phys. Rev. B* 2005, **71**, 155108

34. P. Jaque; A.V. Marenich; C.J. Cramer; D.G. Truhlar, *J. Phys. Chem. C*. 2007, **111**, 5783

35. P. Winget; E.J. Weber; C.J. Cramer; D.G. Truhlar, *Phys. Chem. Chem. Phys*. 2000, **2**, 1231

36. P. Winget; C.J. Cramer; D.G. Truhlar, *Theor Chem Acc*. 2004, **112**, 217

37. J. Ali-Torres; L. Rodriguez-Santiago; M. Sodupe, *Phys. Chem. Chem. Phys*. 2011, **13**, 7852

38. J.A. Bogart; A.J. Lewis; M.A. Boreen; H.B. Lee; S.A. Medling; P.J. Carroll; C.H. Booth; E.J. Schelter, *Inorg. Chem*. 2015, **54**, 2830

39. M. Mazloum-Ardakani; H. Beitollahi; H. Farrokhpour; A.K. Hoshroo, *Iranian Journal of Mathematical Chemistry*. 2012, **3**, 103

40. K. Ambroziak; Z. Rozwadowski; T. Dziembowskaa; B. Bieg, *J. Mol. Struct*. 2002, ***615***, 109

41. W. Schilf ; B. Kołodziej; E. Grech, *J. Mol. Struct.* 2006, **791**, 93

42. A. Adem Cinarli; D. Gürbüz; A. Tavman; A.S. Birteksöz, *Bull. Chem. Soc. Ethiop*. 2011, **25**, 407

43. T. Dziembowska; K. Ambroziak ; I. Majerz, *J. Mol. Struct.* 2005, **738**, 15

44. D.H. Waldeck, *Chem. Rev.* 1991, **91**, 415

45. M. Yildiz; H. Ünver; D. dem Erdener; A. Kiraz; N.O. Iskeleli, *J. Mol. Struct.* 2009, **919**, 227

46. W. Schilf W; B. Kamien ; Z. Rozwadowski ; K. Ambroziak; B. Bieg; T. Dziembowska, *J. Mol. Struct.* 2004, **700**, 61

47. A. Carreño; S. Ladeira; A. Castel; A. Vega; I. Chávez, *Acta Crystallogr.* 2012, **E68**, o2507

48. C.T. Zeyrek; G. Alpaslan; H. Alyar; M. Yıldız; N. Dilek; H. Ünver, *J. Mol. Struct.* 2015, **1088**, 14

49. E. Tozzo; S. Romera; M.P. dos Santos; M. Muraro; R.H. Santos; L.M. Liao; L. Vizotto; E.R. Dockal, *J. Mol. Struct*. 2008, **876**, 110

50. O. Güngör; P. Gürkan, *J. Mol. Struct*. 2014, **107**, 62

51. T. Karatsu; A. Kitamura; H. Zeng; T. Arai; H. Sakuragi; K. Tokumara, *Bull. Chem. Soc. Jpn*. 1995, **68**, 920

52. R.V. Gopal; A.M. Reddy; V.J. Rao, *J. Org. Chem*. 1995, **60**, 7966

53. R.T. Boere; T.L: Roemmele, *Coord. Chem. Rev*. 2000, **210**, 369

54. J. Dokic; M. Gothe; J. Wirth; M.V. Peters; S. Hecht; P. Saalfrank, *J. Phys. Chem. A.* 2009, **113**, 6763

55. F. Leyssner; S. Hagen ; L. Ovari; P. Tegeder, *J. Phys. Chem. C*, 2010, **114**, 1231

56. J. Garcia-Amorós; A. Sanchez-Ferrer ; D. Velasco, *Phys. Chem. Chem. Phys.*, 2010, **12**, 13238

57. J. Lewinski; J. Zachara.; I. Justyniak; M. Dranka, *Coord. Chem. Rev*. 2005, **249**, 1185

58. H. Shekaari; A. Kazempour ; M. Khoshalhan, *Electrochim. Acta* 2014, **147**, 360

60.H.J. Salavagione; J. Arias; P. Garces; E. Morallon; C. Barbero; J.L. Vazquez, *J. Electroanal. Chem.* 2004, **565**, 375

61. H.J. Salavagione; J. Arias-Pardilla; J.M. Perez; J.L. Vazquez; E. Morallon; M.C. Miras; C. Barbero, *J. Electroanal. Chem*. 2005, **576***,* 139

62. P.K. Chattaraj; H. Lee; R.G. Parr, *J. Am. Chem. Soc*. 1991, **113**, 1856

63. A.A. Isse; A. Gennaro ; E. Vianello, *Electrochim. Acta* 1997, **42**, 2065

64. S. Zolezzi; E. Spodine; A. Decinti, *Polyhedron* 2002, **21**, 55

65. L. Méjanelle; J.F. Lòpez; N. Gunde-Cimerman; J.O. Grimalt, *Journal of Lipid Research*, 2001, **42**, 352

66. K. Czaczyk; K. Trojanowska; B. Stachowiak, *Polish Journal of Environmental Studies*. 2002, **11**, 593

67. A.A. Abou-Hussein; W. Linert, *Spectrochimica acta Part A, Molecular and biomolecular spectroscopy.* 2015. **141**, 223

68. A.M. Seyfarth; H.C. Wegener; N. Frimodt-Møller, *Journal of Antimicrobial Chemotherapy*. 1997, **40**, 67

69. A. Deepa; B.J. Nair; T. Sivakumar; A.P. Joseph, *Journal of oral and maxillofacial pathology*. 2014, **18**, 235

70. M.H. Patel; A.M. Patel; S.M. Patel; G.L. Ninama; K.R. Patel; B.C. Lavingia, *National Journal of Community Medicine*. 2011, **2**, 302

71. M. Arvanitis; T. Anagnostou; B.B. Fuchs; A.M. Caliendo; E. Mylonakis, *Clinical microbiology reviews*. 2014, **27**, 490

72. K. Ferreira-Paim; L: Andrade-Silva ; D.J. Mora; E. Lages-Silva; A.L. Pedrosa; P.R. da Silva et al., M*ycopathologia*. 2012, **174**, 41

73. A.J. Bava; R. Negroni., *Rev. Int. Med. Trop. S. Paulo*. 1989, **31**, 346

74. O. López-Jodra; J. M. Torres-Rodríguez; R. Méndez-Vásquez; E. Ribas-Forcadell; Y. Morera-López; T. Baró-Tomás; C. Alia-Aponte, *Journal of Antimicrobial Chemotherapy*, 2000, **45**, 645

75. P. Haddadi ; S. Zareifar ; P. Badiee ; A. Alborzi ; M. Mokhtari; K. Zomorodian ; K. Pakshir ; H. Jafarian. *Jundishapur J. Microbiol.* 2014 , **7**, e11858.

76. J. Heeres; L. Meerpoel; P. Lewi, *Molecules*, 2010, **15**, 4129

77. A. Carreño, M. Gacitua, E. Schott, X. Zarate, J.M. Manriquez, M. Preite, S. Ladeira, A. Castel, N. Pizarro, I. Chavez, R. Arratia-Perez, *New Journal of Chemistry*, 2015, **39**, 5725